



## RESEARCH ARTICLE

10.1029/2018JA026026

## The Formation of an Oxygen Wave by Magnetic Reconnection

P. Tenfjord<sup>1</sup> , M. Hesse<sup>1,2</sup> , and C. Norgren<sup>1</sup> <sup>1</sup>Birkeland Centre For Space Science, University of Bergen, Bergen, Norway, <sup>2</sup>Southwest Research Institute, San Antonio, TX, USA

## Key Points:

- Oxygen density striations forming as oxygen population in inflow is captured by reconnection process
- Quasi-steady accelerated oxygen is trapped in potential well, and develops into layers of high density
- Wavefront-like striations (oxygen density wave) form as a result of Hall electric field developing into the inflow region

## Supporting Information:

- Text S1
- Movie S1

## Correspondence to:

P. Tenfjord,  
paul.tenfjord@ift.uib.no

## Citation:

Tenfjord, P., Hesse, M., & Norgren, C. (2018). The formation of an oxygen wave by magnetic reconnection. *Journal of Geophysical Research: Space Physics*, 123, 9370–9380. <https://doi.org/10.1029/2018JA026026>

Received 22 AUG 2018

Accepted 13 OCT 2018

Accepted article online 5 NOV 2018

Published online 22 NOV 2018

©2018. The Authors.

This is an open access article under the terms of the Creative Commons Attribution-NonCommercial-NoDerivs License, which permits use and distribution in any medium, provided the original work is properly cited, the use is non-commercial and no modifications or adaptations are made.

**Abstract** Oxygen of ionospheric origin is a ubiquitous particle species in magnetospheric dynamics. We investigate how an oxygen population influences magnetic reconnection and how it is energized, using particle-in-cell simulations. The oxygen population is inserted initially in the inflow region, at two equal distances above and below the current sheet, and as time evolves it is captured by the reconnection process. Three simulations with different initial oxygen temperature are investigated. As the oxygen gets involved, layers of high-oxygen density forms in a region bounded by the Hall electric field. These density striations consist of a quasi-steady horizontal layer and a dynamic, inclined, wavefront-like layer. The acceleration of the oxygen population is dominated by electric forces, as the oxygen remains approximately demagnetized for the relevant timescales of the simulation. We describe two mechanisms of oxygen acceleration that lead to these two different structures.

## 1. Introduction

Magnetic reconnection, or merging, describes the process facilitating the release of stored electromagnetic energy into mechanical (kinetic and thermal) energy. The process allows plasma to flow across boundaries separating topologically different classes of magnetic fields (separatrices) by means of a localized violation of the ideal frozen-in condition (Vasyliunas, 1975). Magnetic reconnection plays a crucial role in energy transfer at Earth's dayside magnetopause and in the magnetotail, as well as in solar flares and coronal heating on the Sun (Yamada et al., 2010).

Magnetic reconnection relies on the presence of a dissipation mechanism in a localized region called the diffusion region. The electron diffusion region (EDR) is a region of size  $c/\omega_{pe}$  in which the electrons are not magnetized. The EDR is embedded in the ion diffusion region of size  $c/\omega_{pi}$ , which defines the region where the ions are not magnetized. Inside the EDR, dissipative processes generate electric fields, which lead to the decoupling between the plasma and the magnetic field, a requirement for changing the topological configuration. Understanding the physics in the EDR has traditionally attracted a lot of attention (e.g., Cai et al., 1994; Cai & Lee, 1997; Divin et al., 2010; Fujimoto & Sydora, 2009; Hesse et al., 1999; Lyons & Pridmore-Brown, 1990; Speiser, 1970; Vasyliunas, 1975) but is not the focus of this study.

In addition to protons and electrons, many plasma systems also include heavier species (e.g., André & Cully, 2012). Multispecies plasma in the magnetosphere has been observed by numerous authors using polar orbiting spacecrafts (see Yao & André, 1997, for a review), IMP-7 (Frank et al., 1977), Geotail (e.g., Cohen et al., 1998; Kasahara et al., 2008; Wilken et al., 1995; Zong et al., 1998), Cluster (e.g., Kistler & Mouikis, 2016), and Magnetospheric Multiscale (MMS; e.g., Toledo-Redondo et al., 2016). Of particular interest for magnetospheric dynamics is  $O^+$  of ionospheric origin. In situ observations have shown that the  $O^+$  content of the ring current increases during geomagnetic storms (e.g., Grande et al., 2003; Moore et al., 2001). This suggests that oxygen is captured by magnetotail reconnection and accelerated earthward. Spacecraft observation shows that the density of oxygen in the plasma sheet can be the dominating ion species during storm time conditions (André & Cully, 2012; Kistler et al., 2005, 2006; Kistler & Mouikis, 2016; Mouikis et al., 2010). The source of the magnetotail oxygen is outflow from the high-latitude ionosphere, and higher geomagnetic activity increases the outflow rate (Baker et al., 1982). This suggests that the ionosphere can be a significant source of magnetospheric plasma, especially during storm time conditions, and that participation of mixed populations in reconnection is the common state, rather than the exception. Magnetic reconnection involves the energy conversion of the total mass, momentum, magnetic flux, and energy transport. Understanding how heavier species can influence the reconnection process is important to understand the complete dynamics.

Heavy ions like  $O^+$  has larger Larmor radii than  $H^+$  ions at the same velocities. This leads to a different kinetic behavior and additional scale lengths in the system (Divin et al., 2016; Liu et al., 2014, 2015; Shay & Swisdak, 2004; Toledo-Redondo et al., 2015, 2016). The presence of heavy ions can, if magnetized, mass load the system, and the resulting reduction of the Alfvén velocity is believed to be a mechanism that can slow down or even make reconnection stop (Hesse & Birn, 2004; Karimabadi et al., 2011; Liang et al., 2016; Markidis et al., 2011; Shay & Swisdak, 2004). Using Cluster measurements, Lindstedt et al. (2010) observed  $O^+$  energization by strong localized electric fields at the boundary between the lobe and cusp. These electric fields were related to a reconnection separatrix region and the Hall electric field. The authors argued that this was a source of keV  $O^+$  ions in the magnetosphere. Wang et al. (2014) studied magnetopause reconnection in the presence of hot magnetospheric  $O^+$  observed by Cluster. The authors analyzed the velocity distribution functions for  $O^+$  and  $H^+$  separately and showed that the  $O^+$  are picked up and follow the reconnection outflow. The authors also showed that the velocity of the picked-up oxygen depends on location at which they enter the exhaust. Using multifluid simulations, Winglee and Harnett (2011) found that oxygen can play a crucial role for the development of substorms, as oxygen-enriched lobe field lines convect toward the plasma sheet and reconnect. Liang et al. (2017) showed in a recent paper that oxygen can cross directly from the lobes to downstream of the dipolarization fronts through acceleration by the Hall electric field.

In this study we use a 2.5-D fully kinetic particle-in-cell three-species simulation to study how the oxygen is captured from the lobes by the reconnection process. We show that structured density layers form as the particles are trapped in a potential well created by the Hall electric field. We also show the existence of a density wave, formed as the Hall electric field expands into the lobe region where the oxygen population exists. We describe the motion of the particles constituting the trapped population and the particle motions forming the oxygen wave. We present distribution functions that can be used to compare our findings with observation from the MMS spacecraft.

## 2. Simulation Setup

Our simulation is designed to mimic the magnetotail conditions during enhanced geomagnetic activity. During such conditions, ionospheric outflow from high latitudes enriches the magnetospheric lobes with cold oxygen. Ions originating from the ionosphere are expected to be cold, where observations range from 100 eV (Wygant et al., 2005) up to 260 eV (Seki et al., 1998). In comparison, plasma sheet protons typically have temperatures of a several kiloelectron volts.

We employ a 2.5-D (two spatial components and three fields and velocity coordinates) particle-in-cell simulation, which has previously been applied to a variety of reconnection problems (e.g., Hesse et al., 2001). The initial magnetic field configuration is a two-dimensional generalized Harris-type equilibrium (see Hesse & Birn, 2004, for details) with zero guide field. The initial magnetic field is defined as  $B_x = B_0 \tanh(z/\lambda)$ , where  $\lambda = 2d_i$  is the half width of the layer.

A uniformly distributed proton ( $H^+$ ) background of  $n_b = 0.2$  is added to the Harris-sheet density distribution. In addition to the uniform  $H^+$  population, an oxygen population with number density  $n_o = 0.1$  is added to the inflow region (*lobes*). The oxygen is inserted outside of the current sheet at  $|z| > 2.5d_i$ , henceforth referred to as the initial oxygen boundary. The oxygen population has initially zero bulk and thermal velocity. Thus, initially, the central current sheet consists of protons only, which represent an important difference to other studies where the oxygen population is inserted as a uniform background. All calculations use a proton/electron mass ratio of  $m_p/m_e = 25$  and oxygen/ion mass ratio of  $m_o/m_p = 16$ . A total of  $1.5 \times 10^8$  macroparticles are employed, divided such that  $n_e = n_H + n_o$  is fulfilled. Boundary conditions are periodic at  $x = 0$  and  $x = x_{max}$ . We employ specular reflection for particles at the upper and lower boundaries, and the out-of-plane electric field is set to zero, implying flux conservation in the simulation domain.

Lengths are normalized to the proton inertial length:  $d_i = c/\omega_{pi} (= c\sqrt{\frac{m_i}{4\pi n_i e^2}})$ . Time is normalized to inverse of the proton cyclotron period:  $\Omega_i^{-1} (= \frac{cm_i}{eB})$ . Our simulation domain size is  $200 \times 50d_i$ , and the grid size is  $3, 200 \times 1, 600$ . A time step of  $\omega_e \delta t = 1$  is employed. The velocity normalization is the proton Alfvén speed, based on the foreground current sheet density  $n_o$ , and the electrostatic potential is consequently measured in units of  $\Phi_0 = V_A B_0 c/\omega_{pi}$ , where  $B_0$  is the magnetic field unit. The foreground temperatures fulfill  $T_i + T_e = 0.5$  and proton/electron temperature  $T_i/T_e = 5$ . The ratio between the electron plasma frequency and gyrofrequency is  $\omega_{pe}/\Omega_{ce} = 2$ . In addition to this baseline run, two runs with finite oxygen temperature are explored. The

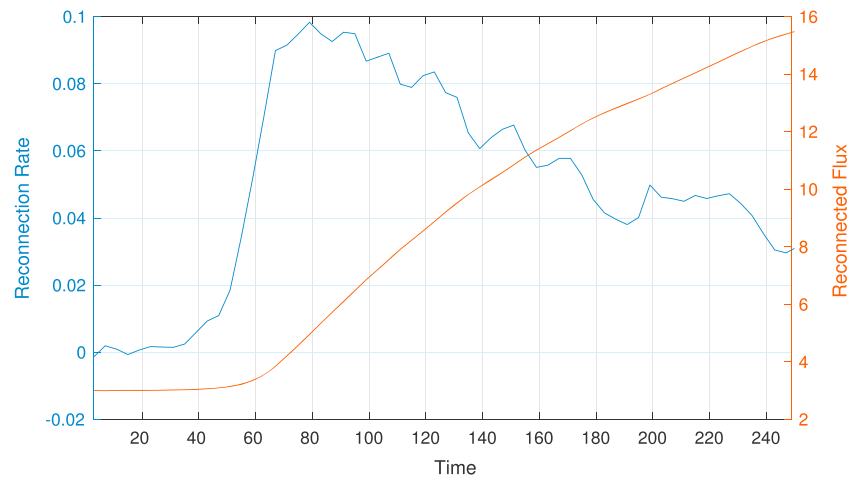


**Figure 1.** Left axis shows the reconnection rate as function of time. Rate of reconnected flux is defined as  $\frac{d}{dt}\Phi_{rec} = \frac{d}{dt} \int \vec{B} \cdot \vec{n} da (= \int E_z dz)$ . The reconnection rate is normalized to the foreground current sheet density. The right axis shows the amount of reconnected flux.

simulation setups are similar, with the only difference being the initial temperature. A comparison between the runs is discussed in section 6.

We study how oxygen is captured by the reconnection process, starting from a current sheet consisting of hydrogen plasma only, and oxygen initially at rest outside our defined oxygen boundary. Magnetic reconnection initiates without the involvement of oxygen, and as time progress, the oxygen participate in the reconnection processes.

### 3. Formation of Oxygen Density Striations

In Figure 2 we show the evolution of the oxygen density and the magnetic field at four different times.  $t = 4$  represents the configuration close to the start of the run, where the oxygen is present in the inflow region only. In Figure 1 we show the evolution of the reconnected magnetic flux and the reconnection rate. The fast phase of reconnection begins around  $t = 48$ , reaching its peak rate at  $t = 80$ . After this the rate drops gradually due to reduced magnetic flux in the inflow region along with a smaller contribution from the back pressure generated by the magnetic island.

At  $t = 72$  we start to observe structures forming in the oxygen density in the inflow region (Figure 2). Oxygen is still not involved in the reconnection process directly. At  $t = 100$ , oxygen has become involved, and horizontal layers of increased density have formed above and below the X-line. Inclined layers of increased density have formed to the left and right of the reconnection region. These structures are propagating away from the reconnection region as seen at  $t = 120$ . Also note the regions of almost zero oxygen density behind the propagating tilted layers.

There is a significant difference in how the striations form close to the X-line and how they form, evolve, and grow in the outflow region. The horizontal density layers are a consequence of quasi-steady flow of oxygen into the reconnection region from the inflow region (preacceleration). The inclined layers produce what we call an *oxygen density wave*, which forms as a consequence of the localized Hall  $E_z$  field growing and expanding into regions where the oxygen is at rest. We will now discuss the mechanism of these two processes separately.

#### 3.1. Preaccelerated Oxygen Population

We first discuss the oxygen population that is preaccelerated in the inflow region. The term *preaccelerated* is used here to describe the relatively slow z-directed oxygen velocity in the inflow region. This flow arises as the reconnection process initiates flux transport in the inflow region directed toward the X-point. The agile electrons move with the field, while the  $O^+$  cannot keep up. An ambi-polar (charge-separation) field accelerates the oxygen to preserve charge quasi-neutrality. Eventually, the initial  $H^+$  plasma in the plasma sheet is ejected, and fresh multispecies ( $O^+$  and  $H^+$ ) lobe flux replenishes the plasma sheet (Karimabadi et al., 2011; Liang et al., 2016).

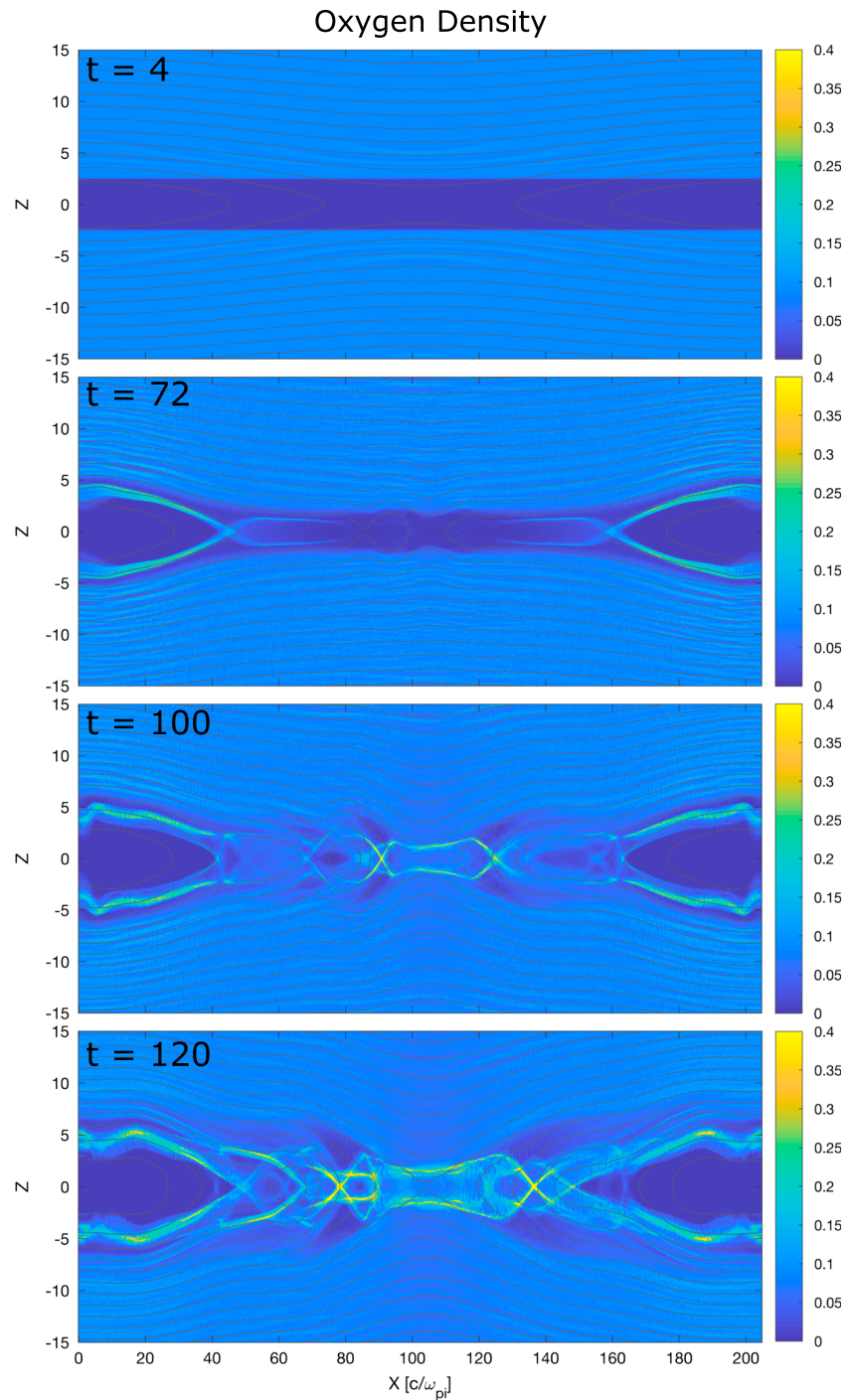


**Figure 2.** Oxygen density as foreground and magnetic field as background at four different stages of the evolution; see text for details.

In Figure 3 we show four different particle trajectories, originating from two different locations (white circles). The top panels show the oxygen density, and the bottom panels show the electric field  $E_z$ . All panels have particle trajectories overlaid, where the colors represent the in-plane ( $x - z$ ) particle velocity. The particle trajectories are calculated by first extracting velocity distribution functions from the region highlighted by the white circles at time  $t = 108$ . From the distributions we extract the representative velocities and trace oxygen test particles forward and backward in time in the dynamically changing fields. The distribution functions will be discussed in section 4.1

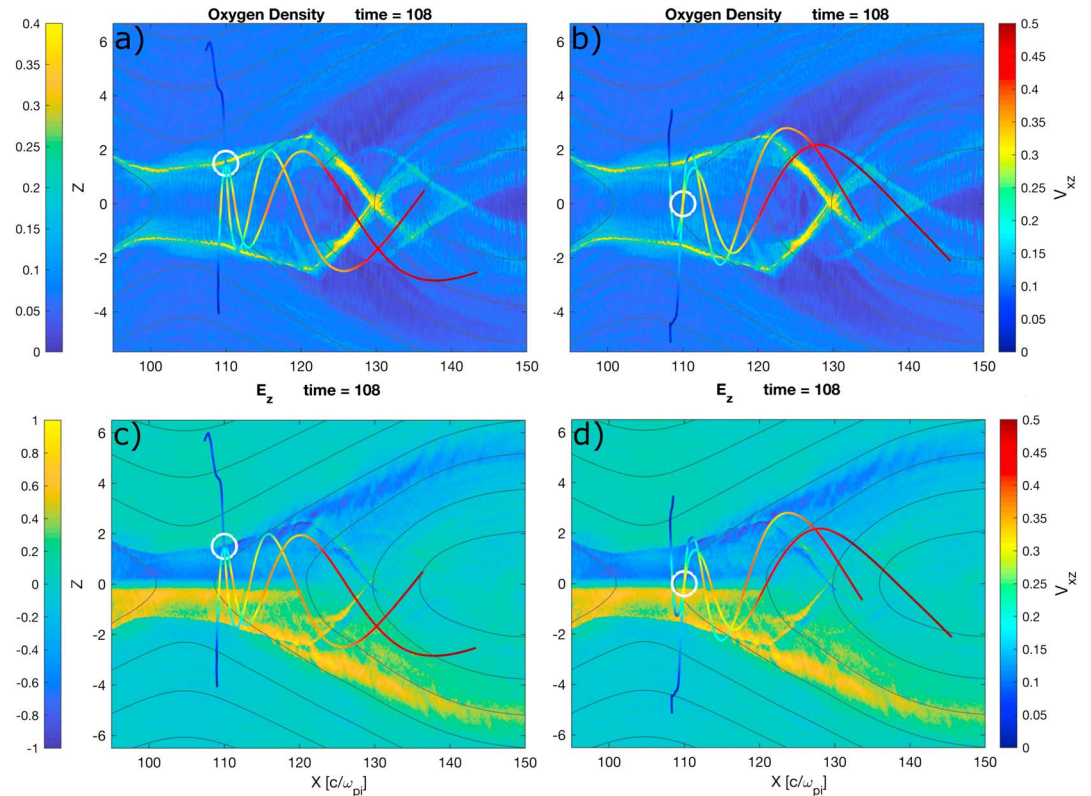


**Figure 3.** Oxygen density and Hall electric field with four particle trajectories. Panels (a) and (c) show the trajectory of two particles passing through the density striation. Panels (b) and (d) show two particles passing through the center, where both are trapped. See text for details.

All the particles in Figure 3 are coming in from the inflow region with a small velocity. The color-coded particle trajectories show that the particles have a minimum velocity as they are reflected and therefore spend a longer time at that region, contributing to the density striation layer. The time between the start of the trajectory and the white circle, and from the white circle to the end, represents  $100 \Omega_i^{-1}$  each. In panels (a) and (c) the particle ensemble consists of one population passing straight through the northern density striation and one population that gets reflected. Panels (b) and (d) show two particle populations passing through the current sheet. The particle with the smallest  $v_x$  represents a particle accelerated directly from the southern inflow region, while the second particle has been reflected once. For oxygen with higher temperature the striation layer is more smeared out owing to their thermal velocity; see section 5.

As the particles reach the Hall  $E_z$  field, they experience direct ballistic acceleration across the associated potential drop (see Figure 3). The magnitude of the potential drop is such that an oxygen with mass  $m_o$  accelerated through the potential drop will increase its kinetic energy by  $\Phi_0 = 1/2 m_o v_o^2$ , where  $\Phi_0$  is the integral of  $E_z$  (which is the gradient of a potential in good approximation). To estimate the maximum velocity along  $x = 110$ , we integrate  $E_z$  from  $z = -1.73$  to  $z = 0$ . This gives us a potential  $\Phi \approx 27$ , which estimates the velocity of an oxygen ion to  $v_o = 0.36$ . As soon as the oxygen particle gains significant velocity through the acceleration by the electric field, it starts to experience the Lorentz force, although the dynamics is still dominated by the electric field (see Figure 5). This deflects the particle primarily to the  $y$ -direction through  $v_z \cdot B_x$ . Thus, the estimated velocity ( $v_z = 0.36$ ) is slightly higher than the  $v_z$  velocity seen in the velocity distribution function (section 4.1) since part of the  $v_z$  gained by electric field acceleration is deflected into  $v_x$  and  $v_y$ . This prevents the particle from escaping the potential well. The forces acting on the particles will be discussed in section 4.

The maintenance of the horizontal density layers close to the current sheet requires fresh oxygen particles from the inflow region. The transport of fresh oxygen particles from the inflow region depends on the reconnection rate, and for this reason the magnitude of the density layers varies in time, dissipating as the

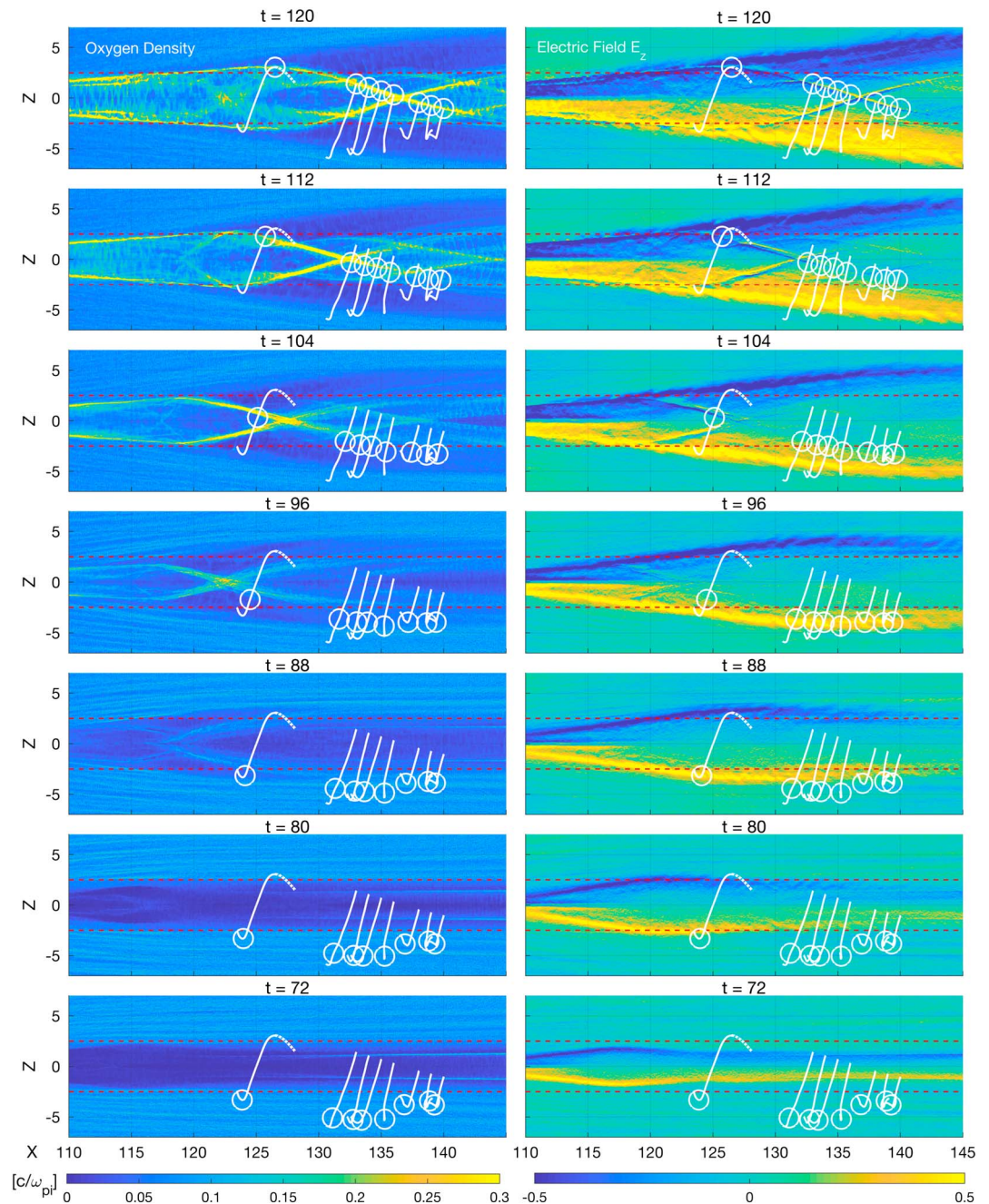


**Figure 4.** Formation of oxygen wave: oxygen density and Hall electric field  $E_z$  at different times with multiple particle trajectories overlain. See text for details.

reconnection process ceases. The oxygen particles do generally not undergo more than three to four bounces. At this point the particles have gained a too large  $v_x$  to participate in maintaining the striations.

Protons and electrons show similar density profiles due to their meandering motion (e.g., Fujimoto, 2006; Speiser, 1965). However, the oxygen striations does not form as a consequence of magnetic interaction, but instead, the oxygen is accelerated by the Hall electric field, and bouncing in the potential well.

The behavior of the oxygen population is similar to the dynamics of cold protons in the outflow inferred from Cluster observations by Wygant et al. (2005). Also, in a simulation result by Divin et al. (2016), the authors found cold ions were accelerated by the Hall electric field and performed bouncing motions in the electric potential well, indicating a trapped population similar to what we observe.

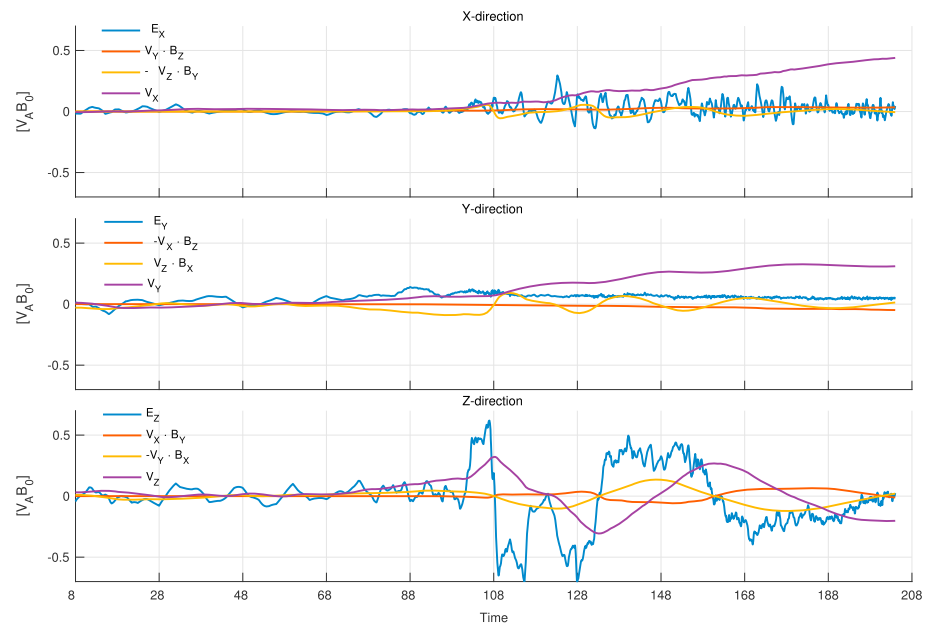


**Figure 5.** Forces acting on particle coming in from the southern lobe in Figure 3b. Velocities extracted from velocity distribution at  $t = 108$  shown in Figure 6b. The particle is traced backward ( $t < 108$ ) and forward ( $t > 108$ ) in time from this location.

### 3.2. Oxygen Wave From Evolving Hall $E_z$

The quasi-steady description of how oxygen gets trapped in the potential well can only describe the horizontal layers above and below the X-line. How the striations grows in time (Figure 2) requires a dynamic description, as it depends on how the localized electric fields evolve as reconnection proceeds.

In Figure 4 we show the oxygen density and the Hall  $E_z$  electric field at different times. The apparent cross structure represents interpenetration of two interactionless fronts. We focus on the the density front propagating in the positive  $z$ -direction. We extracted velocity distribution functions along this density structure. These locations are shown as white circles in Figure 4 at  $t = 120$ . The trajectories are traced backward from this initial location to determine their origin, starting from velocities of large phase space density. At each time step, the circle denote where the particles are at the time of the plot. The dashed red horizontal lines at  $z = 2.5$  and  $z = -2.5d_i$  show where the oxygen population exists at the start of the simulation. At  $t = 72$ , the traced particles are all sitting outside our initial oxygen boundary ( $2.5 < z < -2.5$ ), and the Hall electric field has not yet reached the population. At  $t = 80$ ,  $E_z$  has evolved and expanded out to the oxygen boundary. Although not yet reaching the particles we trace, it shows how the Hall electric evolves outward, eventually crossing the oxygen boundary. At the next time step shown ( $t = 88$ ),  $E_z$  has reached our leftmost particle and is now accelerating the available oxygen in the positive  $z$ -direction. This becomes even clearer in the next time step ( $t = 96$ ). Now,  $E_z$  has expanded slightly farther and is now reaching the rest of the trajectories. At the leftmost trajectory, the acceleration of the available oxygen has left behind a wake of almost zero oxygen density. Due to the low-oxygen temperature the evacuation of the oxygen population from this region does not produce an appreciable back pressure, so that the population outside the reach of  $E_z$  remains unaffected. At  $t = 104$  the leftmost particle is traveling along with the *wavefront* and reaches its maximum velocity. For the remaining particles, the wavefront is forming ahead of the Hall  $E_z$ , and a clear  $x$ -directed velocity gradient is visible. At  $t = 112$ , the leftmost particle has been decelerated but not yet reflected. The remaining particles have all been accelerated, and are now propagating as a wavefront, leaving a wake of nearly zero oxygen density behind. At this time, the Hall electric field does not expand significantly but instead increases in magnitude. However, the particles that occupied this region have already been accelerated. In the top panel, the leftmost particle gets reflected. This is illustrated by the dashed line, which represents the trace of the particle forward in time. Thus, this shows how the oxygen wave straightens and explains how the horizontal density striations expands in the  $x$ -direction. At this time the rightmost particle reaches or has reached its maximum velocity. These particles will also, at a later time, be reflected by the negative Hall electric field.

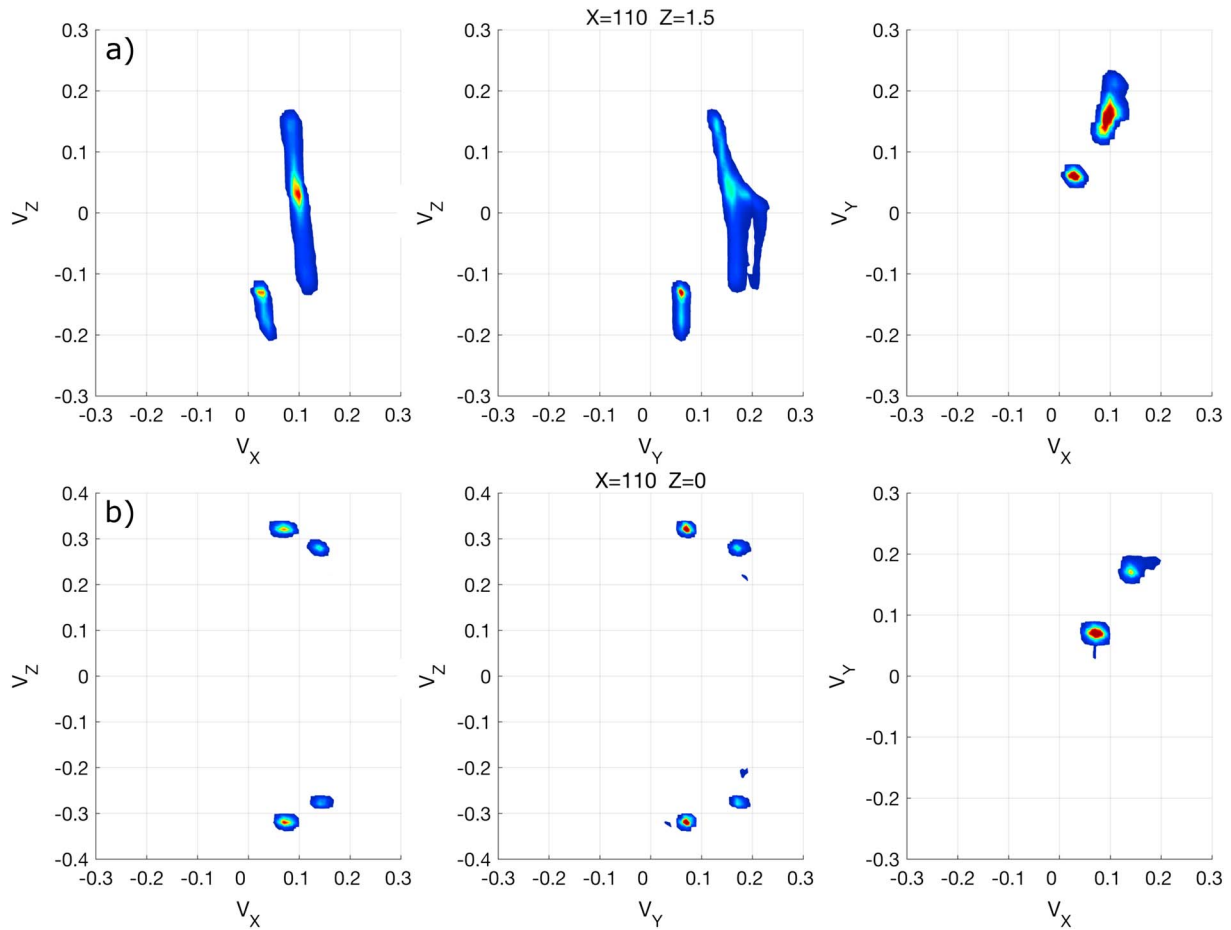


**Figure 6.** Velocity distribution functions from two white circles in Figure 3. Panel (a) shows two classes of particles, where the smeared-out distribution represents particles that have been or are about to be reflected. The colder distribution represents the particles coming in from the northern lobe and pass straight through the density striation. In panel (b) the particle ensemble consists of four different velocities. Between the striations the particles have their highest velocity. The particles that have gained the largest  $v_x$  have been bounced once, and some of their  $v_z$  velocity has been diverted into  $v_x$  and  $v_y$ .

To summarize, we have described that the formation of the horizontal striations occurs at the location where the in-plane velocity is at a minimum, that is, at the location, where oxygen bounces in the electrostatic potential. On the other hand, the wavefront density peak travels with the velocity of the oxygen. The cross structure represents the intersection of two wavefronts, which do not interact with each other significantly.

In section 5, we will show that the oxygen wave also forms when the oxygen has a finite temperature.

#### 4. Particle Distribution and Forces

To understand the time history and the forces acting on the oxygen particles, we show the forces acting on a representative particle as a function of time. Figure 5 shows forces acting on the particle coming in from the southern lobe in Figure 3b. The particle velocity is extracted from the velocity distribution at time  $t = 108$ , shown in Figure 6b (the distribution with the highest positive  $v_z$ ). The top panel shows the forces acting in the  $x$ -direction. The particle experiences a fluctuating  $E_x$ , which is on average positive (for  $t > 103$ ), accelerating the particle in the positive  $x$ -direction. The initial  $v_x$  acceleration (at  $t = 103$ ) is given primarily by  $-v_z \cdot B_y$ , following the ballistic acceleration in the  $z$ -direction by the Hall electric field. The contribution from  $v_y \cdot B_z$  and  $E_x$  forces the particle in the  $x$ -direction, while  $-v_z \cdot B_y$  enhances or reduces  $v_x$  based on the sign of  $v_z$  and the Hall magnetic field.

In the  $y$ -direction we see a steady increase of  $v_y$ . This is due to acceleration by  $E_y$  in the diffusion region. The electric field dominates the evolution with a contribution from  $v_z \cdot B_x$ , reducing or enhancing  $v_y$  depending on the location of the particle.

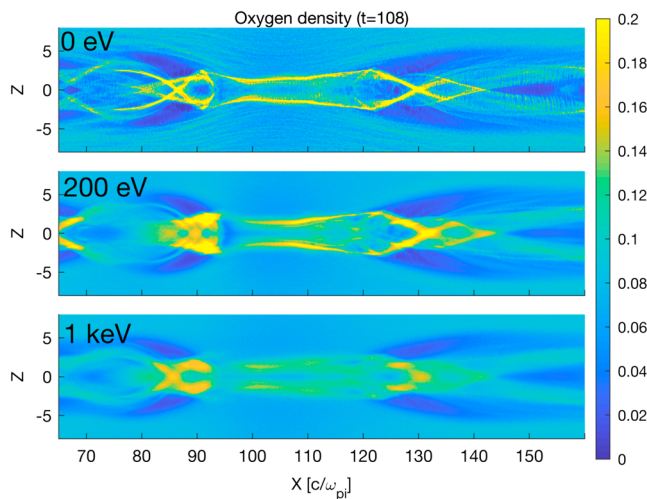


**Figure 7.** Oxygen density striations for three different initial temperatures: (a) cold oxygen population, (b) 200 eV, and (c) 1 keV. This shows that density striation can be expected to form for all realistic oxygen temperatures (magnetotail) originating from ionospheric outflow.

For the z-direction the evolution is again dominated by the electric field. As a result of the acceleration by  $E_y$ , the resulting magnetic force ( $-v_y \cdot B_x$ ) is in the same direction as the Hall  $E_z$  (yellow and blue lines in bottom panel in Figure 5). During the first bounces the electric force clearly dominates. At the end the magnetic force becomes comparable to the Hall electric field, and here Speiser-like confinement becomes more important (Speiser, 1965). It is the acceleration by  $E_y$  and the resulting  $-v_y \cdot B_x$  that contribute to keeping the oxygen confined in the Hall potential well.

#### 4.1. What Would In Situ Measurements Find?

In order to predict what in situ observation by MMS or Cluster would show, we show the oxygen velocity distribution functions from the two locations highlighted in Figure 3. Figure 6a shows the velocity distributions taken at the upper density striation (Figures 3a and 3c). The velocity distribution shows two classes of particles. The colder population is cold oxygen from the northern inflow region accelerated by Hall  $E_z$  in the negative z-direction. This corresponds to the particle passing through the density striation in Figure 3a. The second population has a much larger spread in velocities, as it consists of a mix of particles not yet reflected (positive  $v_z$ ) and particles that have been reflected (negative  $v_z$ ).

At the center of the current sheet (Figure 6b) we have four classes of particles. The particles have their maximum velocity at this location. The particles with the highest  $v_z$  velocity are coming straight in from the inflow regions, while the two populations with lower  $|v_z|$  and higher  $v_x$  have bounced once, signifying that they have lost some of their z-momentum and gained x-momentum.

Signatures of counterstreaming oxygen have been reported in both simulations (Liu et al., 2015) and observed using Cluster (Wygant et al., 2005). The authors also present distribution functions showing signatures of trapped oxygen populations.

## 5. Simulations With Finite Initial Temperature

We have so far discussed how the cold oxygen population is captured by the reconnection process and how striations form. While the  $O^+$  population in the magnetotail has been observed to be cold, zero thermal velocity must be considered as an extreme. As discussed in the introduction, the expected temperature of  $O^+$  ions in the magnetotail is between 100 and 300 eV (Seki et al., 1998; Wygant et al., 2005). To determine the effect of a finite temperature, two more simulations with 200-eV and 1-keV  $O^+$  were executed. These scaled temperatures correspond to a 2% for 200-eV and 10% for 1-keV reduction of the proton temperature compared to the baseline run to preserve pressure balance in the simulations. The 1-keV simulation can be regarded as an upper extreme. Figure 7 shows the  $O^+$  density at  $t = 108$  for the three simulations. While the striations are most prominent for the cold run, they are clearly seen in the simulations with temperature included. We therefore expect that these striations might be visible for all realistic magnetotail  $O^+$  temperatures.

## 6. Discussion and Summary

We have investigated how a cold oxygen population is captured by the reconnection process. The oxygen population with initially vanishing velocity or temperature does not get appreciably magnetized inside the diffusion region. Instead, the oxygen was found to be accelerated in a ballistic way when the Hall electric field either evolves into the background population or as preaccelerated oxygen reaches the Hall field. The preaccelerated particles are responsible for the horizontal density striations above and below the diffusion region. The evolution of these particles is dominated by electric forces, with a weaker contribution from the Lorentz force, which reduces the in-plane velocity and therefore keeps the particles trapped in the potential well. We also showed that as the Hall electric field evolves into the background oxygen population, it accelerates the oxygen such that it resembles a wavefront. We called this the oxygen wave. Evidence of  $O^+$  acceleration in reconnection has been reported in both simulations and observations (Liang et al., 2017; Lindstedt et al., 2010;

Liu et al., 2015; Wygant et al., 2005). Our results provide a detailed prediction of oxygen structures, which should be observable by magnetospheric missions.

It is possible that such structures have been seen before by Wu et al. (2016), who observed a thin structure of enhanced  $O^+$  density embedded in magnetotail proton current sheet using the Cluster spacecraft. The authors found this structure to have a scale size comparable to the local reconnection current sheet and to be isolated from the larger scale size associated with  $O^+$ .

In the simulation we have shown how an oxygen population initially at rest is captured by the reconnection process and ejected in the outflow directions. Although the oxygen remains demagnetized in the timescale of the simulation, and it does not participate directly in the reconnection dynamics, it still suggests that the oxygen extracts energy from the process. The energy spent on the oxygen population is thus not accessible for the  $H^+$  population, and a reduction of the reconnection rate will be unavoidable. Hesse and Birn (2004) and Markidis et al. (2011) ran a similar simulations without observing significant decrease in the reconnection rate; however, their simulation domain was much smaller. We therefore suggest that a significant decrease in the reconnection rate will be observed if the simulation domain includes the extended regions, where the majority of oxygen can, in fact, be accelerated. This cannot be resolved/confirmed in the present paper but will be the topic of further investigation.

### Key Findings

We have showed how oxygen density striations form as an oxygen population in the inflow region (lobes) is captured by the reconnection process.

- When an oxygen population located in the lobes is captured by the reconnection process density striations can form.
- The oxygen population is accelerated in a ballistic way when (1) a preaccelerated population reaches the Hall electric field or (2) when the Hall electric field reaches the oxygen population.
- The preaccelerated oxygen population results in quasi-steady horizontal density striations, where a relatively small contribution from the Lorentz force reduces the in-plane velocity, keeping the oxygen particles trapped in the Hall potential well.
- The oxygen wave forms as a consequence of the localized Hall  $E_z$  field growing and expanding into regions where the oxygen is at rest.
- As the reconnection rate gradually is reduced due to annihilation of magnetic flux, the inflow of fresh lobe oxygen is reduced, and the horizontal bands weakens in magnitude.
- Simulations with finite temperature shows that the striations are more smeared out for higher initial temperature but should be visible for all realistic magnetotail  $O^+$  temperatures.
- The oxygen dynamics is dominated by electric forces. As the oxygen is demagnetized on the relevant reconnection timescales it acts almost like test particles—albeit acting as an energy sink on the finite energy reservoir—and therefore may indirectly affect the reconnection electric field.
- Distribution functions consist of dense phase space blobs with different spread depending on the history of the particles. Particles with more complicated history lead to smeared-out distributions.

### References

- André, M., & Cully, C. M. (2012). Low-energy ions: A previously hidden solar system particle population. *Geophysical Research Letters*, *39*, L03101. <https://doi.org/10.1029/2011GL050242>
- Baker, D. N., Hones, E. W., Young, D. T., & Birn, J. (1982). The possible role of ionospheric oxygen in the initiation and development of plasma sheet instabilities. *Geophysical Research Letters*, *9*(12), 1337–1340. <https://doi.org/10.1029/GL009i012p01337>
- Cai, H. J., Ding, D. Q., & Lee, L. C. (1994). Momentum transport near a magnetic X line in collisionless reconnection. *Journal of Geophysical Research*, *99*(A1), 35–42. <https://doi.org/10.1029/93JA02519>
- Cai, H. J., & Lee, L. C. (1997). The generalized Ohm's law in collisionless magnetic reconnection. *Physics of Plasmas*, *4*(3), 509–520. <https://doi.org/10.1063/1.872178>
- Cohen, C. S., Galvin, A. B., Ipavich, F. M., Kol, Y., Lui, A. T. Y., Lundgren, R. A., et al. (1998). Concurrent observations of solar wind oxygen by Geotail in the magnetosphere and wind in interplanetary space. *Geophysical Research Letters*, *25*(15), 2987–2990.
- Divin, A., Khotyaintsev, Y. V., Vaivads, A., André, M., Toledo-Redondo, S., Markidis, S., & Lapenta, G. (2016). Three-scale structure of diffusion region in the presence of cold ions. *Journal of Geophysical Research: Space Physics*, *121*, 12,001–12,013. <https://doi.org/10.1002/2016JA023606>
- Divin, A., Markidis, S., Lapenta, G., Semenov, V. S., Erkaev, N. V., & Biernat, H. K. (2010). Model of electron pressure anisotropy in the electron diffusion region of collisionless magnetic reconnection. *Physics of Plasmas*, *17*(12), 122102. <https://doi.org/10.1063/1.3521576>
- Frank, L. A., Ackerson, K. L., & Yeager, D. M. (1977). Observations of atomic oxygen ( $O^+$ ) in the Earth's magnetotail. *Journal of Geophysical Research*, *82*(1), 129–134.
- Fujimoto, K. (2006). Time evolution of the electron diffusion region and the reconnection rate in fully kinetic and large system. *Physics of Plasmas*, *13*(7), 72904. <https://doi.org/10.1063/1.2220534>

### Acknowledgments

This study was supported by the Research Council of Norway/CoE under contract 223252/F50 and by the NASA MMS project. Data available upon request.

- Fujimoto, K., & Sydora, R. D. (2009). Particle description of the electron diffusion region in collisionless magnetic reconnection. *Physics of Plasmas*, 16(11), 112309. <https://doi.org/10.1063/1.3263694>
- Grande, M., Perry, C. H., Hall, A., Fennel, J., Nakamura, R., & Kamide, Y. (2003). What is the effect of substorms on the ring current ion population during a geomagnetic storm? In A. Surjalal Sharma, Y. Kamide & G. S. Lakina (Eds.), *Disturbances in Geospace: The Storm-Substorm Relationship* (Vol. 142). American Geophysical Union. <https://doi.org/10.1029/142GM08>
- Hesse, M., & Birn, J. (2004). On the cessation of magnetic reconnection. *Annales Geophysicae*, 22, 603–612.
- Hesse, M., Kuznetsova, M., & Birn, J. (2001). Particle-in-cell simulations of three-dimensional collisionless magnetic reconnection. *Journal of Geophysical Research*, 106(A12), 29831. <https://doi.org/10.1029/2001JA000075>
- Hesse, M., Schindler, K., Birn, J., & Kuznetsova, M. (1999). The diffusion region in collisionless magnetic reconnection. *Physics of Plasmas*, 6(5), 3–23. <https://doi.org/10.1063/1.873436>
- Karimabadi, H., Roytershteyn, V., Mouikis, C. G., Kistler, L. M., & Daughton, W. (2011). Flushing effect in reconnection: Effects of minority species of oxygen ions. *Planetary and Space Science*, 59(7), 526–536. <https://doi.org/10.1016/j.pss.2010.07.014>
- Kasahara, S., Hasegawa, H., Keika, K., Miyashita, Y., Nishino, M. N., Sotirelis, T., et al. (2008). Escape of high-energy oxygen ions through magnetopause reconnection under northward IMF. *Annales Geophysicae*, 26, 3955–3966.
- Kistler, L. M., & Mouikis, C. G. (2016). The inner magnetosphere ion composition and local time distribution over a solar cycle. *Journal of Geophysical Research: Space Physics*, 121, 2009–2032. <https://doi.org/10.1002/2015JA021883>
- Kistler, L. M., Mouikis, C. G., Cao, X., Frey, H., Klecker, B., Dandouras, I., et al. (2006). Ion composition and pressure changes in storm time and nonstorm substorms in the vicinity of the near-Earth neutral line. *Journal of Geophysical Research*, 111, 1–12. <https://doi.org/10.1029/2006JA011939>
- Kistler, L. M., Mouikis, C., Mόbius, E., Klecker, B., Sauvaud, J. A., Rόme, H., et al. (2005). Contribution of nonadiabatic ions to the cross-tail current in an O<sup>+</sup> dominated thin current sheet. *Journal of Geophysical Research*, 110, A06213. <https://doi.org/10.1029/2004JA010653>
- Liang, H., Ashour-Abdalla, M., Lapenta, G., & Walker, R. J. (2016). Oxygen impacts on dipolarization fronts and reconnection rate. *Journal of Geophysical Research A: Space Physics*, 121, 1148–1166. <https://doi.org/10.1002/2015JA021747>
- Liang, H., Lapenta, G., Walker, R. J., Schriver, D., El-Alaoui, M., & Berchem, J. (2017). Oxygen acceleration in magnetotail reconnection. *Journal of Geophysical Research: Space Physics*, 122, 618–639. <https://doi.org/10.1002/2016JA023060>
- Lindstedt, T., Khotyaintsev, Y. V., Vaivads, A., Andrό, M., Nilsson, H., & Waara, M. (2010). Oxygen energization by localized perpendicular electric fields at the cusp boundary. *Geophysical Research Letters*, 37, L09103. <https://doi.org/10.1029/2010GL043117>
- Liu, Y. H., Kistler, L. M., Mouikis, C. G., Roytershteyn, V., & Karimabadi, H. (2014). The scale of the magnetotail reconnecting current sheet in the presence of O<sup>+</sup>. *Geophysical Research Letters*, 41, 4819–4827. <https://doi.org/10.1002/2014GL060440>
- Liu, Y. H., Mouikis, C. G., Kistler, L. M., Wang, S., Roytershteyn, V., & Karimabadi, H. (2015). The heavy ion diffusion region in magnetic reconnection in the Earth's magnetotail. *Journal of Geophysical Research: Space Physics*, 120, 3535–3551. <https://doi.org/10.1002/2015JA020982>. Received
- Lyons, L. R., & Pridmore-Brown, D. C. (1990). Force balance near an X line in a collisionless plasma. *Journal of Geophysical Research*, 95(A12), 20, 903. <https://doi.org/10.1029/JA095iA12p20903>
- Markidis, S., Lapenta, G., Bettarini, L., Goldman, M., Newman, D., & Andersson, L. (2011). Kinetic simulations of magnetic reconnection in presence of a background O<sup>+</sup> population. *Journal of Geophysical Research*, 116, 1–13. <https://doi.org/10.1029/2011JA016429>
- Moore, T. E., Chandler, M. O., Giles, B. L., Delcourt, D. C., Horwitz, J. L., & Pollock, C. J. (2001). Ring currents and internal plasma sources. *Space Science Reviews*, 95, 555–568.
- Mouikis, C. G., Kistler, L. M., Liu, Y. H., Klecker, B., Korth, A., & Dandouras, I. (2010). H<sup>+</sup> and O<sup>+</sup> content of the plasma sheet at 15–19 Re as a function of geomagnetic and solar activity. *Journal of Geophysical Research*, 115, 1–12. <https://doi.org/10.1029/2010JA015978>
- Seki, K., Terasawa, T., Hirahara, M., & Mukai, T. (1998). Quantification of tailward cold O<sup>+</sup> beams in the lobe/mantle regions with Geotail data: Constraints on polar O<sup>+</sup> outflows. *Journal of Geophysical Research*, 103(A12), 29,371–29,381. <https://doi.org/10.1029/98JA02463>
- Shay, M. A., & Swisdak, M. (2004). Three-species collisionless reconnection: Effect of O<sup>+</sup> on magnetotail reconnection. *Physical Review Letters*, 93(17), 4–7. <https://doi.org/10.1103/PhysRevLett.93.175001>
- Speiser, T. W. (1965). Particle trajectories in model current sheets: 1. Analytical solutions. *Journal of Geophysical Research*, 70(17), 4219–4226. <https://doi.org/10.1029/JZ070i017p04219>
- Speiser, T. W. (1970). Conductivity without collisions or noise. *Planetary and Space Science*, 18(4), 613–622. [https://doi.org/10.1016/0032-0633\(70\)90136-4](https://doi.org/10.1016/0032-0633(70)90136-4)
- Toledo-Redondo, S., Andrό, M., Khotyaintsev, Y. V., Vaivads, A., Walsh, A., Li, W., et al. (2016). Cold ion demagnetization near the X-line of magnetic reconnection. *Geophysical Research Letters*, 43, 6759–6767. <https://doi.org/10.1002/2016GL069877>
- Toledo-Redondo, S., Vaivads, A., Andrό, M., & Khotyaintsev, Y. V. (2015). Modification of the Hall physics in magnetic reconnection due to cold ions at the Earth's magnetopause. *Geophysical Research Letters*, 42, 6146–6154. <https://doi.org/10.1002/2015GL065129>
- Vasyliunas, V. M. (1975). Theoretical models of magnetic field line merging, 1. *Reviews of Geophysics and Space Physics*, 13(1), 303–336. <https://doi.org/10.1029/RG013i001p0303>
- Wang, S., Kistler, L. M., Mouikis, C. G., Liu, Y. H., & Genestreti, K. J. (2014). Hot magnetospheric O<sup>+</sup> and cold ion behavior in magnetopause reconnection: Cluster observations. *Journal of Geophysical Research: Space Physics*, 119, 9601–9623. <https://doi.org/10.1002/2014JA020402>. Received
- Wilken, B., Zong, Q. G., Daglis, I. A., Doke, T., Livi, S., Maezawa, K., et al. (1995). Tailward flowing energetic oxygen ion bursts associated with multiple flux ropes in the distant magnetotail: GEOTail observations. *Geophysical Research Letters*, 22(23), 3267–3270. <https://doi.org/10.1029/95GL02980>
- Winglee, R. M., & Harnett, E. (2011). Influence of heavy ionospheric ions on substorm onset. *Journal of Geophysical Research*, 116, A11212. <https://doi.org/10.1029/2011JA016447>
- Wu, T., Fu, S. Y., Zong, Q. G., Sun, W. J., Cui, Y. B., Zhao, D., et al. (2016). Thin energetic O<sup>+</sup> layer embedded in the magnetotail reconnection current sheet observed by Cluster. *Geophysical Research Letters*, 43, 11,493–11,500. <https://doi.org/10.1002/2016GL071184>
- Wygant, J. R., Cattell, C. A., Lysak, R., Song, Y., Dombeck, J., Mcfadden, J., et al. (2005). Cluster observations of an intense normal component of the electric field at a thin reconnecting current sheet in the tail and its role in the shock-like acceleration of the ion fluid into the separatrix region. *Journal of Geophysical Research*, 110, 1–30. <https://doi.org/10.1029/2004JA010708>
- Yamada, M., Kulsrud, R., & Ji, H. (2010). Magnetic reconnection. *Reviews of Modern Physics*, 82(1), 603–664. <https://doi.org/10.1103/RevModPhys.82.603>
- Yao, A. W., & Andrό, M. (1997). Sources of ion outflow in the high latitude ionosphere. *Space Science Reviews*, 80, 1–25.
- Zong, Q. G., Wilken, B., Woch, J., Mukai, T., Yamamoto, T., Reeves, G. D., et al. (1998). Energetic oxygen ion bursts in the distant magnetotail as a product of intense substorms: Three case studies. *Journal of Geophysical Research*, 103(A), 20,339–20,364. <https://doi.org/10.1029/97JA01146>